Journal of Marine Science and Technology

Volume 31 | Issue 4 Article 6

Bearing Capacity Factor Characteristics of Footings on Double-Layered Cohesive Soils

Chao-Ming Chi
Dept. of Civil Engineering, Feng Chia University, Taichung (407802), Taiwan, cmchi@mail.fcu.edu.tw

Zheng-Shan Lin
Ph.D. Program for Infrastructure Planning and Engineering, Feng Chia University, Taichung (407), Taiwan

Yu-Shu Kuo
Dept. of Hydraulic and Ocean Engineering, National Cheng Kung University, Tainan (701), Taiwan

Recommended Citation

Chi, Chao-Ming; Lin, Zheng-Shan; and Kuo, Yu-Shu (2023) "Bearing Capacity Factor Characteristics of Footings on Double-Layered Cohesive Soils," *Journal of Marine Science and Technology*: Vol. 31: Iss. 4, Article 6.
DOI: 10.51400/2709-6998.2713
Available at: https://jmstt.ntou.edu.tw/journal/vol31/iss4/6

RESEARCH ARTICLE

Bearing Capacity Factor Characteristics of Footings on Double-layered Cohesive Soils

Chao-Ming Chi [a,*], Zheng-Shan Lin [b], Yu-Shu Kuo [c]

[a] Dept. of Civil Engineering, Feng Chia University, Taichung, 407802, Taiwan
[b] Program for Infrastructure Planning and Engineering, Feng Chia University, Taichung, 407, Taiwan
[c] Dept. of Hydraulic and Ocean Engineering, National Cheng Kung University, Tainan, 701, Taiwan

Abstract

In this study, the bearing capacity of a surface foundation resting on a double-layered cohesive soil profile was investigated by applying a rotational mechanism and finite-difference numerical simulations. The bearing capacity factor behaviors of a surface footing on double-layered cohesive soils can be classified and illustrated using a characteristic chart. Depending on the soil strata strength ratio and normalized layer thickness, the soil-foundation system can be in the squeezing, factor-increasing, factor-decreasing, or constant factor zones. The results indicated that the trend of the curves in the characteristic chart computed from the asymmetric failure mechanism was in accordance with that of the symmetric failure mechanism of the numerical simulation. Based on the strength conditions of the upper and lower soil layers, the soil plastic flow zone may enlarge, shrink, or even become constrained. For the analysis of the critical soil strength ratio that causes punching shear failure, the results from the SNAME method were less conservative. Moreover, the footing roughness effect was significant in the weaker upper soil case and may have contributed to a 25 % higher bearing capacity.

Keywords: Offshore foundations, Bearing factor characteristic, Numerical modelling, Footing roughness, Failure mechanism, Layered soils

1. Introduction

Offshore oil, & gas, and offshore wind account for much of the offshore development. With the development of engineering technologies, offshore oil and gas platforms are being employed in nearshore to offshore deep-water areas. Offshore wind has better power-generating characteristics than onshore wind; therefore, wind energy companies are becoming increasingly interested in offshore wind power [1]. The first offshore wind farm, Vindeby, located in Denmark, was built in 1991 and operates commercially [2]. Taiwan is actively advancing the development and utilization of offshore wind energy as a key policy in its renewable energy strategy [3]to achieve 5.5 GW offshore wind power capacity by 2025 to significantly boost the share of renewable energy [4].

Offshore platforms are widely used in the oil and gas industry, and some can be adapted to offshore wind turbines [5]. The environmental loads of offshore structures are greater than those of onshore buildings, which generally results in larger dimensions of offshore foundations [6]. The first gravity-based platform, Ekofisk I, was installed in the Norwegian sector of the Central North Sea in 1973; the equivalent radius of its foundation area was approximately 97 m [7]. Furthermore, jack-up barges are commonly utilized to construct offshore wind farms, and the dimensions of the spudcan footings can reach or exceed 20 m [5], as shown in Fig. 1. Therefore, the range of soils affected by large offshore foundations under loading can extend to significant depths, leading to the inclusion of either a single thick layer or stratified soil [8]. For a relatively small footing placed on nonhomogeneous

Received 19 March 2023; revised 12 October 2023; accepted 14 October 2023.
Available online 15 December 2023

* Corresponding author.
E-mail address: cmchi@mail.fcu.edu.tw (C.-M. Chi).

https://doi.org/10.51400/2709-6998.2713

cohesive soil deposits, inhomogeneity may not have a significant effect on the bearing capacity analysis, and it is sufficiently accurate to apply an average value of the undrained shear strength as a constant [9]. However, for large footings such as offshore foundations and embankments, the nonhomogeneous effect cannot be ignored in the assessment of the bearing capacity.

Notation

B	width of foundation
H	thickness of top layer
H/B	normalized layer thickness
N_c, N_q, N_γ	bearing factors
n	relative strength
$n_{critical}$	critical relative strength
ϕ'	effective stress angle of friction
q_{ult}	ultimate bearing capacity
S_u	undrained shear strength of cohesive soil
$S_{u,bot}$	undrained shear strength of bottom layer soil
$S_{u,top}$	undrained shear strength of top layer soil
$S_{u,bot}/S_{u,top}$	strength ratio

2. Problem definition

Bearing capacity, installation resistance, and settlement evaluation are the primary issues in foundation design. Murff [13] further indicated that estimating the foundation capacity has always been a central issue in foundation analyses and design.

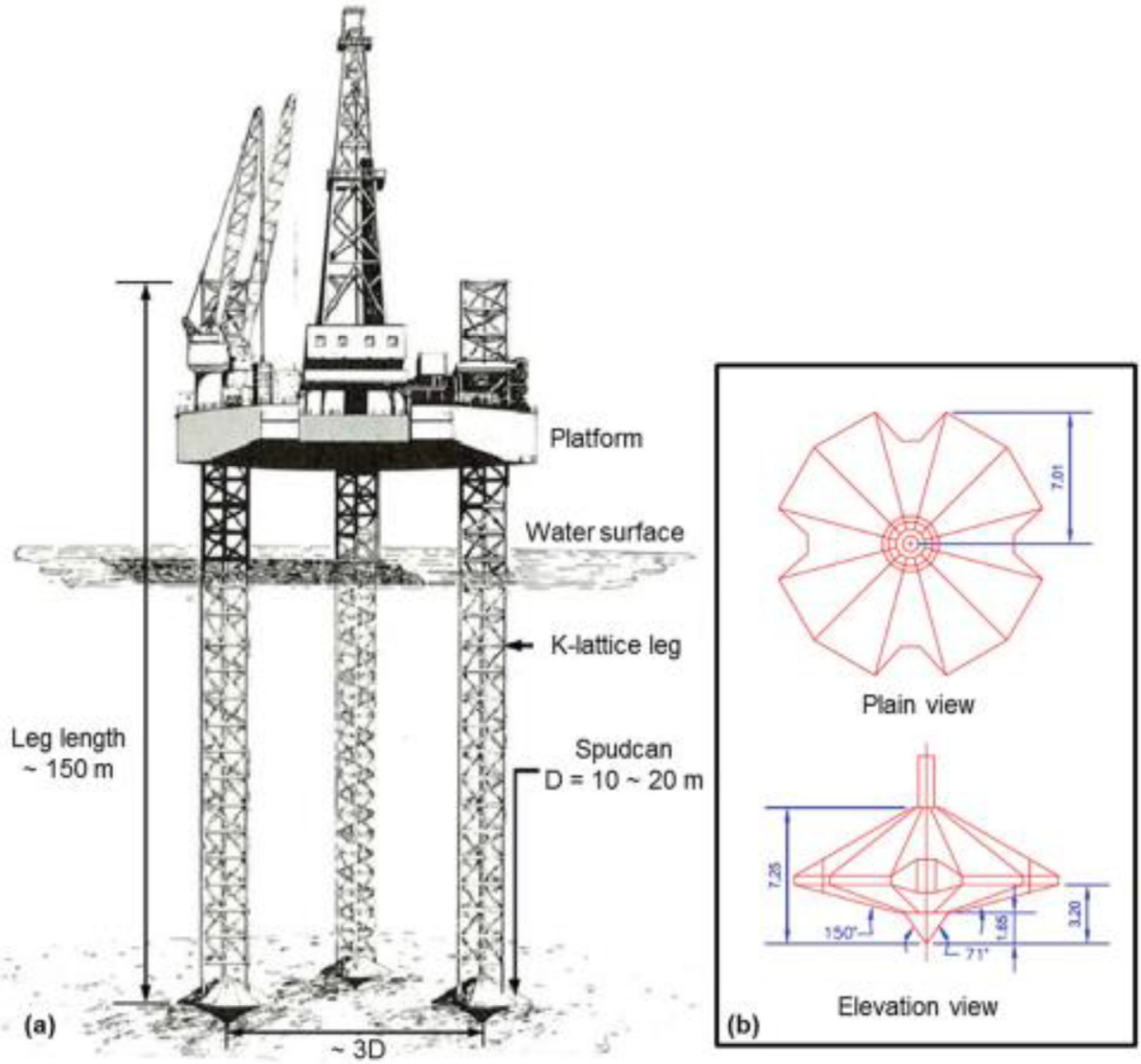

Fig. 1. Typical jack-up vessel and spudcan foundation [10]: (a) whole jack-up rig [11]; (b) spudcan foundation geometry [12].

Fig. 2 shows the common types of offshore structures with shallow foundations and various shapes of offshore shallow foundations. Shallow foundations are considered when the width of the foundation is less than or approximately equal to the depth of embedment [14]. Shallow foundations occasionally become an economic solution as an alternative to deep foundations [6]; however, the dimensions of shallow foundations may become the main consideration. A gravity-based foundation (GBS) is a typical type of shallow foundation that may be up to hundreds of meters or equivalent in diameter. Piled raft systems can serve as suitable solutions, particularly for abutments, piers, and high-rise building foundations, to decrease the foundation dimensions, increase the ultimate bearing capacity, and minimize excessive settlement of foundations [15,16].

Terzaghi [14] provided a theoretical solution to assess the ultimate bearing capacity (q_{ult}) of a rough shallow foundation placed on a homogeneous and isotropic soil layer [17], and the expression is as follows:

$$q_{ult} = cN_c s_c d_c + qN_q s_q d_q + 0.5B\gamma N_\gamma s_\gamma d_\gamma \quad (1)$$

where c is the cohesion in soil, q is surcharge, B is width of foundation, γ is the unit weight of soil, s_c, s_q, and s_γ are shape factors, d_c, d_q, and d_γ are depth factors, and N_c, N_q, and N_γ are bearing capacity factors. Meyerhof [18] indicated that for a surface foundation on a cohesive soil layer, the expression for the bearing capacity is given by the following equation, and it was adopted by the Society of Naval Architects and Marine Engineers (SNAME) [19] to calculate the capacity and penetration of footings of jack-up units:

$$q_{ult} = S_u N_c s_c d_c \quad (2)$$

where s_c is the shape factor, and d_c is the depth factor, which can be obtained using Eq. (3):

$$\begin{cases} s_c = 1 + 0.2K_p \dfrac{B}{L} \\ d_c = 1 + 0.2\sqrt{K_p}\,\dfrac{D_f}{B} \end{cases} \quad (3)$$

where L is the length of the foundation, D_f is the depth of the embedment, and K_p is the Rankine passive earth pressure coefficient. Additionally, Gui and Muhunthan [20] indicated that if the embedment depth is $D_f \neq 0$, then the material density, stress level, roughness of the soil-footing interface, and soil compressibility will affect the ultimate bearing capacity (q_{ult}); therefore, the ultimate bearing capacity (q_{ult}) should be determined directly rather than modifying the bearing capacity factors for surface footings. However, for a surface strip foundation rested on cohesive soil ($\phi' = 0$), the shape factor and the depth factor are $s_c = 1.0$ and $d_c = 1.0$. The bearing capacity theory was originally developed for a strip footing placed on a homogeneous soil surface, and the effect of shape or depth was later considered by multiplying the associated factors. The cohesive bearing factor proposed by Terzaghi [14] is $N_c = 5.71$; however, Prandtl [21] and Hill [22] obtained $N_c = \pi + 2$ for both perfectly smooth and rough foundations on undrained cohesive soil based on the method of characteristics. In other words, the soil-footing interface roughness did not affect the bearing factor while the foundation was set on a homogeneous undrained cohesive soil deposit. Nevertheless, the profiles of the undrained shear strength (S_u) of cohesive soils are

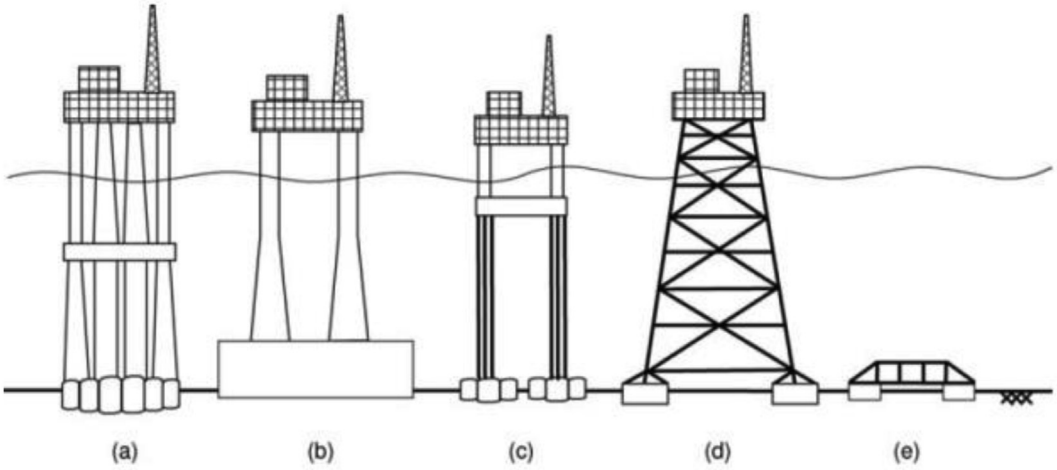

Fig. 2. Applications of offshore shallow foundations: (a) Condeep gravity-based structure (GBS); (b) GBS; (c) Tension-leg platform (TLP); (d) Jacket; (e) Subsea frame [6].

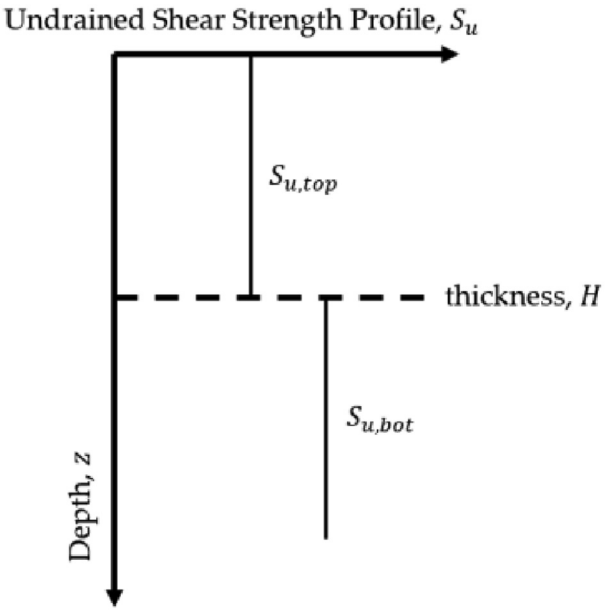

Fig. 3. Variation of $S_{u,top}$ and $S_{u,bot}$ with depth.

generally not homogeneous, leading to significant impacts on the bearing capacity calculation results owing to site-specific conditions [23]. Davis and Booker [9] and Chi and Lin [8] indicated that foundation roughness affects the value of the bearing factor for a nonhomogeneous undrained cohesive soil profile. According to geotechnical investigation data, offshore wind farm sites in Taiwan generally present complex in-situ soil conditions, with soil profiles often characterized by the presence of multiple soil-type strata [24]. Therefore, it is necessary to consider the effect of layered soils on the bearing capacity of a larger foundation. Furthermore, clayey silts show excess pore water pressure during shearing; therefore, undrained shear strength can be employed in the foundation bearing capacity assessment.

Each stratum possesses fairly uniform properties to evaluate the ultimate bearing capacity of a foundation placed on a double-layered cohesive soil profile (Fig. 3). Reddy and Srinivasan [25], Brown and Meyerhof [26], Chen [27], and Merifield et al. [28] obtained the bearing factors using different analysis methods. Brown and Meyerhof [26] suggested semi-empirical bearing capacity factors through a series of laboratory model tests, and Merifield et al. [28] obtained rigorous upper- and lower-bound solutions by numerical limit analysis. To obtain the upper-bound solutions for the ultimate bearing capacity, a mode of foundation failure under a plastic collapse load should be assumed. Reddy and Srinivasan [25] and Chen [27] calculated the upper-bound solutions based on the assumption that failure occurs along a simple circular surface (Fig. 4). The ultimate bearing capacity (q_{ult}) of a footing on a double-layered cohesive soil profile (Fig. 3) was investigated in this study using the rotational mechanism and finite-difference numerical simulations, which can be resolved into three cases: (I) $S_{u,top} = S_{u,bot}$, where the foundation failure mode can be general shear failure; (II) $S_{u,top} < S_{u,bot}$, where squeezing might occur; and (III) $S_{u,top} > S_{u,bot}$, where the failure mechanism may lead to catastrophic punch-through shear failure.

3. Background

3.1. Rotational mechanism

As mentioned above, the bearing capacity theory was originally built for a footing placed on a homogeneous soil deposit, and the effect of the foundation shape or embedment depth was considered by multiplying the associated factors. This study investigated the advanced features of the fundamental bearing capacity (q_{ult}) of a footing on double-layered cohesive soil using a theoretical rotational mechanism and numerical simulation. To evaluate the ultimate bearing capacity of a foundation on double-layered cohesive soils, Reddy and

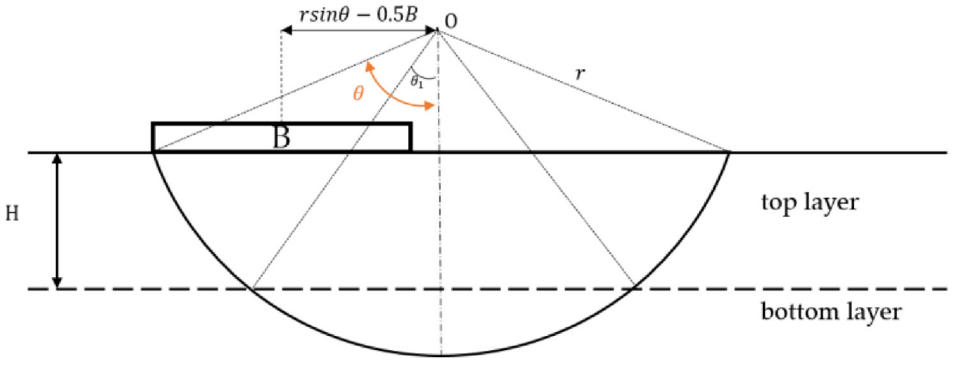

Fig. 4. Schematic diagram of a proposed rotational mechanism.

Srinivasan [25] used the limit equilibrium method, assuming a simple circular failure surface, as shown in Fig. 4, and Chen [27] applied the upper bound method, assuming the same soil flow mechanism. The bearing factor is expressed as follows:

$$N_c = \frac{q_{ult}}{S_{u,top}} = \frac{\left(\frac{r}{B}\right)^2}{\left(\frac{r}{B}\right) sin\,\theta - 0.5} \times (2\theta + 2n\theta_1) \tag{4}$$

where r is the radius of the failure surface, and θ is an angle. n is the relative strength and can be expressed as follows:

$$n = \frac{S_{u,bot}}{S_{u,top}} - 1 \tag{5}$$

and θ_1 can be expressed as follows:

$$\theta_1 = cos^{-1}\left(cos\,\theta + \frac{H}{r}\right) \tag{6}$$

where H is the thickness of the top layer and Eq. (7) is used to obtain the minimum value of Eq. (4):

$$\begin{cases} \dfrac{\partial N_c}{\partial \theta} = 0 \\ \dfrac{\partial N_c}{\partial r} = 0 \end{cases} \tag{7}$$

When the relative strength is $n = 0$, representing a homogeneous condition, Eqs. (4) and (7) can be solved analytically, resulting in $N_c = 5.52$ [8]. The variations of the bearing factor (N_c) with normalized layered thicknesses (H/B) and relative strength (n) is shown in Fig. 5. The following points can be observed from Fig. 5: (I) assuming a constant value for H/B, the value of N_c increases with an increase in relative strength (n) until a critical relative strength ($n_{critical}$) is reached; (II) for the scenarios of $H/B < 0.66$ (dashed-curves), an increment in bearing factors ($N_c > 5.52$) for $S_{u,top} < S_{u,bot}$, with the associated positive critical relative strength ($n_{critical} > 0$); (III) for the cases of $H/B \geq 0.66$ (solid-curves), the bearing factors reach maximum value (5.52), with the associated negative or neutral critical relative strength ($n_{critical} \leq 0$) [8].

3.2. Numerical simulation

Brown and Meyerhof [26], Meyerhof and Hanna [29], and Merifield et al. [28] indicated that the

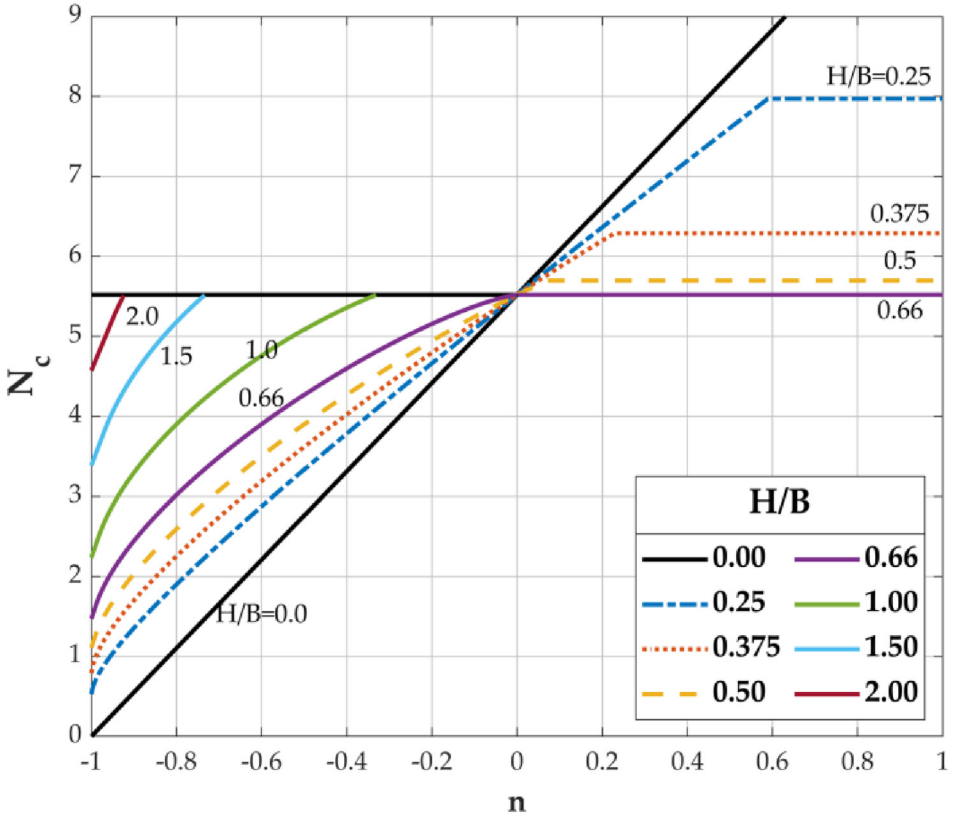

Fig. 5. N_c values with various H/B and n.

Table 1. Parameters applied in FLAC simulations for evaluation bearing capacity.

Parameter	Symbol	Property Value	Reference
Poisson's ratio	υ	0.49	Lambe & Whitman [30]
Young's modulus	E	$500S_u$	Cheng et al. [31]
normalized layer thickness	H/B	$0.25 \sim 2.0$	Brown & Meyerhof [26], Meyerhof & Hanna [29],
strength ratio	$S_{u,bot}/S_{u,top}$	$0.2 \sim 2.0$	and Merifield et al. [28]

bearing capacity of a foundation on double-layered cohesive soils was primarily affected by the normalized layer thickness (H/B) and strength ratio ($S_{u,bot}/S_{u,top}$). Moreover, Brown and Meyerhof [26] showed that an increment in bearing factor for $S_{u,bot}/S_{u,top} > 1$ occurs up to $H/B \cong 0.7$, and the bearing capacity would not be affected by subsequent layers for $S_{u,bot}/S_{u,top} < 1$ when $H/B \geq 3.0$.

Lambe and Whitman [30] indicated that Poisson's ratio (υ) is $\upsilon = 0.5$ for undrained loading, and Bulk Modulus (K) can be expressed as follows:

$$K = \frac{E}{3(1-2\upsilon)} \tag{8}$$

where E is the Young's modulus. While Poisson's ratio approaches $\upsilon \rightarrow 0.5$, the associated Bulk Modulus (K) would be approaching infinity. Therefore, Poisson's ratio is set as $\upsilon = 0.49$ and the Young's modulus of cohesive soils is set to $E = 500S_u$ [31]. The ranges of the normalized layer thickness (H/B), strength ratio ($S_{u,bot}/S_{u,top}$), and soil parameters imposed in the FLAC numerical simulations are listed in Table 1. Additionally, the plane strain condition and the Mohr-Coulomb Yield criteria with the associated flow rule were utilized in the FLAC numerical simulations. The velocity boundary conditions were specified in the numerical models, and a constant downward velocity was applied to the joints representing the footing, as shown in Fig. 6. Finally, the bearing factor at the numerical load limit is calculated using Eq. (9) [32].

$$N_{c,FLAC} = \frac{\sum f_i^{(y)}}{BS_{u,top}} \tag{9}$$

where $f_i^{(y)}$ is the vertical soil resistance at footing joint i. For $S_{u,bot}/S_{u,top} = 1.0$ representing the homogeneous cohesive soil conditions, the numerical bearing factor obtained in the study of a perfectly rough footing was $N_c = 5.17$ and that of a perfectly smooth footing was $N_c = 5.10$. The error between the numerical results and exact solutions was less than 0.8 %. Merifield et al. [28] obtained numerical upper- and lower-bound solutions for these cases, with average values of 5.13 for a perfectly rough footing and 5.09 for a perfectly smooth footing.

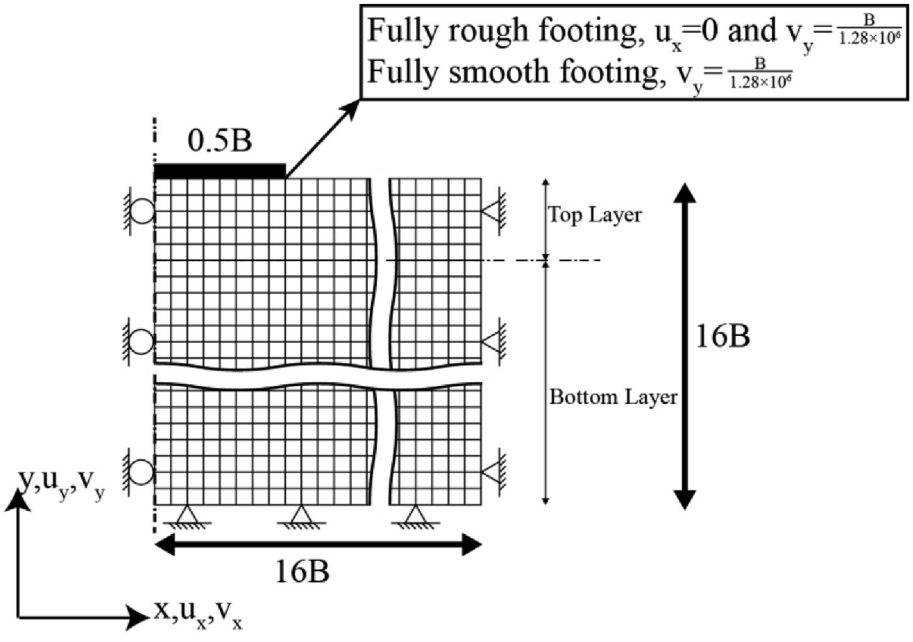

Fig. 6. Numerical simulation model.

Therefore, the confidence in the accuracy of these numerical results from FLAC is given by good agreement with the exact solutions, and the numerical results of the parametric study, covering most of the problems in the possible ranges (Table 1), can then be discussed.

4. Rotational mechanism results

4.1. The bearing factor characteristic behavior

The bearing capacity factors of a surface foundation placed on double-layered cohesive soil can be estimated by assuming a simple circular slip surface. The associated bearing capacity factors can be computed using Eqs. (4) and (7). For the homogeneous case ($n = 0$), the bearing factor was $N_c = 5.52$ determined by the rotational mechanism. However, it varies with the soil strata strength ratio ($S_{u,bot}/S_{u,top}$) and normalized layer thickness (H/B) for $n \neq 0$. Fig. 7 shows the bearing capacity factor surface computed using the rotational mechanism. The value of the bearing factor varies significantly for a smaller normalized layer thickness, especially for $H/B < 0.66$, and it maintains at 5.52 for most larger H/B zones. Fig. 5 shows a side view of the strength ratio, and the curves in the figure are the contours of the bearing factor surface shown in Fig. 7. As mentioned earlier, the phenomenon of increasing the bearing factor ($N_c > 5.52$) is only limited to the intersection zone of $H/B < 0.66$ and n > 0; however, the range of the bearing factor reduction zone can extend to a high normalized layer thickness. The critical relative strength is an important index for judging the variation in the bearing factors, especially for the stability of the foundations under stronger topsoil conditions ($n_{critical} < 0$). Fig. 8 shows the bearing capacity factor characteristics of a footing resting on double-layered cohesive soils, and there are four zones in this chart. The bearing factors in Zones (I) and (II) are greater than 5.52, which is a constant value in Zone (IV) and lower than that in Zone (III). Fig. 8 shows the plan view of the bearing factor surface in Fig. 7; more bearing factors are toward 5.52 once the normalized layer thickness (H/B) is larger than 0.66. The bearing factor value for each specific H/B in Zone (I), the squeezing zone, is a maximum constant; however, it increases as the normalized layer thickness decreases.

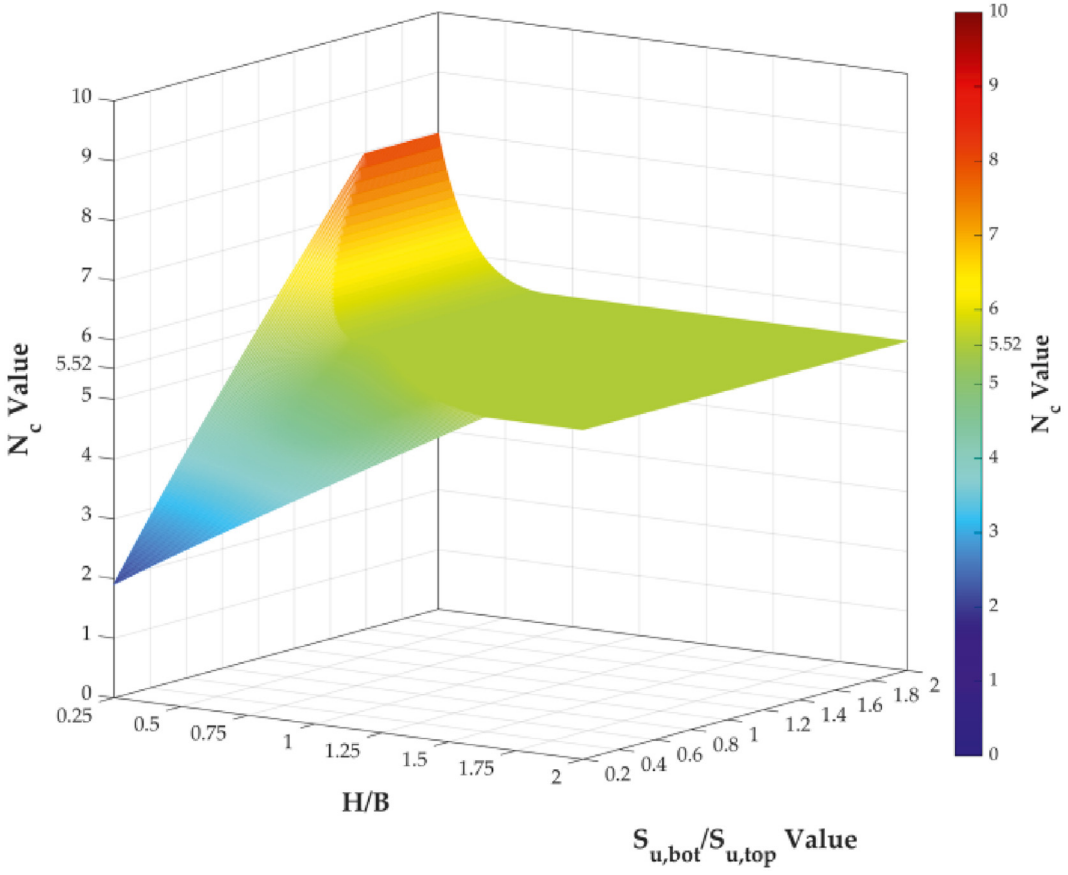

Fig. 7. Bearing factor surface computed from the rotational mechanism.

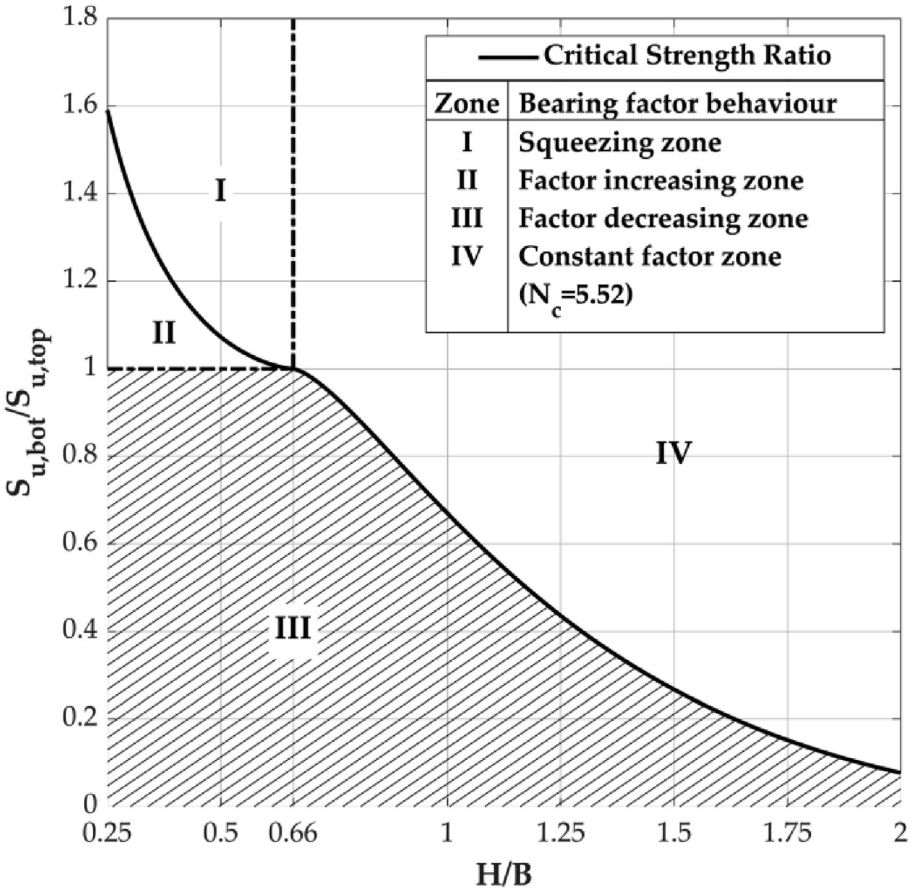

Fig. 8. Double-layered cohesive soils bearing factor characteristic chart.

4.2. $S_{u,bot}/S_{u,top} \leq 1$

All the bearing capacity factors are less than or equal to 5.52 when the bottom layer soil strength was lower than that of the top layer. The curve between Zones (III) and (IV), shown in Fig. 8, indicates the critical strength ratios required for various normalized layer thicknesses to reduce the bearing factors. Fig. 9 compares predicted bearing factors for $S_{u,bot}/S_{u,top} \leq 1$ to test data (23 points) from Brown & Meyerhof [26], and 17 points of them (74 %) fall within the Zone (III) (Factor Decreasing Zone) shown in Fig. 8. The solid curve is identical to the border curve mentioned above, and can be expressed in the following regression form:

$$\left(\frac{S_{u,bot}}{S_{u,top}}\right)_{critical} = \frac{1.7}{(H/B)^4 + 1.5}\ ;\ 0.66 < \frac{H}{B} < 2.0 \qquad (10)$$

The contours and testing data showed that the values of the bearing factors decreased for smaller strength ratio ($S_{u,bot}/S_{u,top}$) and normalized layer thickness (H/B). However, most values of the test data are lower than those predicted from the analysis. In other words, the rotational mechanism tended to overestimate the actual bearing factor. Because the failure surface was assumed to be an arc according to the upper-bound theorem, the determined collapse load was greater than or equal to the exact solution.

4.3. $S_{u,bot}/S_{u,top} \geq 1$

When a footing is placed on a weaker stratum overlying a stronger stratum system ($n \geq 0$), the associated bearing factor would be on the $S_{u,bot}/S_{u,top} \geq 1.0$ side, including Zones (I), (II), and (IV) shown in Fig. 8. For relatively larger normalized layer thickness conditions $H/B \geq 0.66$, the ultimate bearing capacity would be not affected by the bottom stratum soil strength and the associated bearing factors located in Zone (IV) with the constant value $N_c = 5.52$. However, for $H/B < 0.66$ conditions, the bearing capacity would vary with both H/B and $S_{u,bot}/S_{u,top}$, and the associated higher bearing factor ($N_c \geq 5.52$) might belong to Zone (I) or (II). Therefore, the phenomenon of increasing bearing factors exists only under $H/B < 0.66$ and $S_{u,bot}/S_{u,top} > 1$.

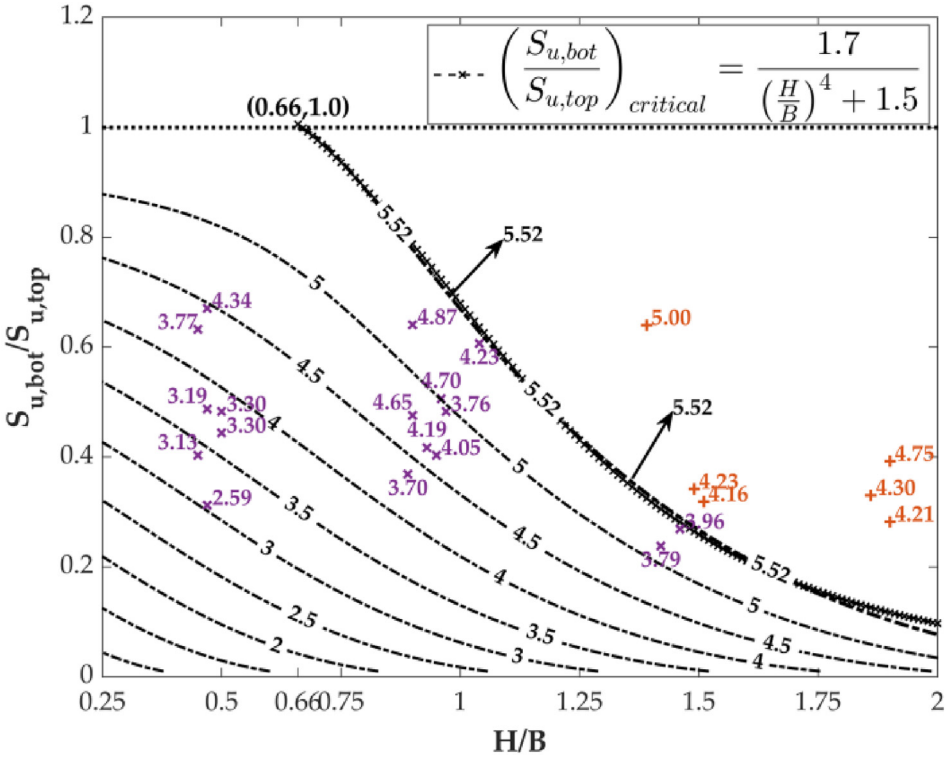

Fig. 9. Contours of the bearing factor surface on $S_{u,bot}/S_{u,top} \leq 1$ side and testing data from Brown & Meyerhof [26].

When the normalized layer thickness remains constant, the strength ratio gradually increases, and the associated bearing factor also increases (Zone II) until it reaches the critical strength ratio (Zone I). This behavior of the bearing factor is shown in Fig. 5. Therefore, the critical strength ratio curve between Zones (I) and (II) shown in Fig. 8 represents the required minimum strength ratios of various normalized layer thicknesses for top-layer soil squeezing.

When the foundation failure mode is squeezing, the associated soil slip circle is fully constrained in the top weaker soil stratum and is tangential to the strata interface [8]. Therefore, the radius of the soil slip arc can be expressed as follows:

$$r = \frac{H}{1 - cos\,\theta} \tag{11}$$

Eq. (11) implies that the angle $\theta_1 = 0$; therefore, the effect of the relative strength (n) vanishes to the bearing factor. Substituting Eq. (11) into Eq. (4), the bearing factor is the function of the variable θ once H/B is determined as follows:

$$N_c = \frac{q_{ult}}{S_{u,top}} = \frac{2\theta\left[\frac{H/B}{(1-cos\,\theta)}\right]^2}{\left[\frac{H/B}{(1-cos\,\theta)}\right] sin\,\theta - 0.5} \tag{12}$$

According to Eq. (12), for the soil-squeezing mode, the associated ultimate bearing capacity (q_{ult}) or bearing factor (N_c) was not affected by the subsequent stratum. Therefore, the bearing factors located in Zone (I) are only affected by the normalized layer thickness (H/B); however, those belonging to Zone (II) would vary with both H/B and the strength ratio ($S_{u,bot}/S_{u,top}$).

The contours of the bearing factors in Zones (I) and (II) are shown in Fig. 10. Furthermore, the solid curve in this figure is identical to the border curve between Zones (I) and (II) shown in Fig. 8 and can be expressed in the following regression form:

$$\left(\frac{S_{u,bot}}{S_{u,top}}\right)_{critical} = \frac{0.08}{(H/B)^{1.6}} + 0.84;\ 0.25 < \frac{H}{B} < 0.66 \tag{13}$$

The bearing factors in Zone (II) are $N_c \geq 5.52$ and vary with H/B and $S_{u,bot}/S_{u,top}$. In contrast, the contour lines of the bearing factors in Zone (I) are parallel to $S_{u,bot}/S_{u,top}$ axis, and their spacing decreases as H/B decreases. The critical strength ratio curve identifies the behavior of the bearing factors and the characteristics of the associated soil failure surface. In Zone (I), the failure slip circle lies entirely within the topsoil stratum, and the failure mode is similar to the case of a footing supported by soil with a rigid base at a limited depth. Shield [33] and Murff [13] proposed the concept of squeezing

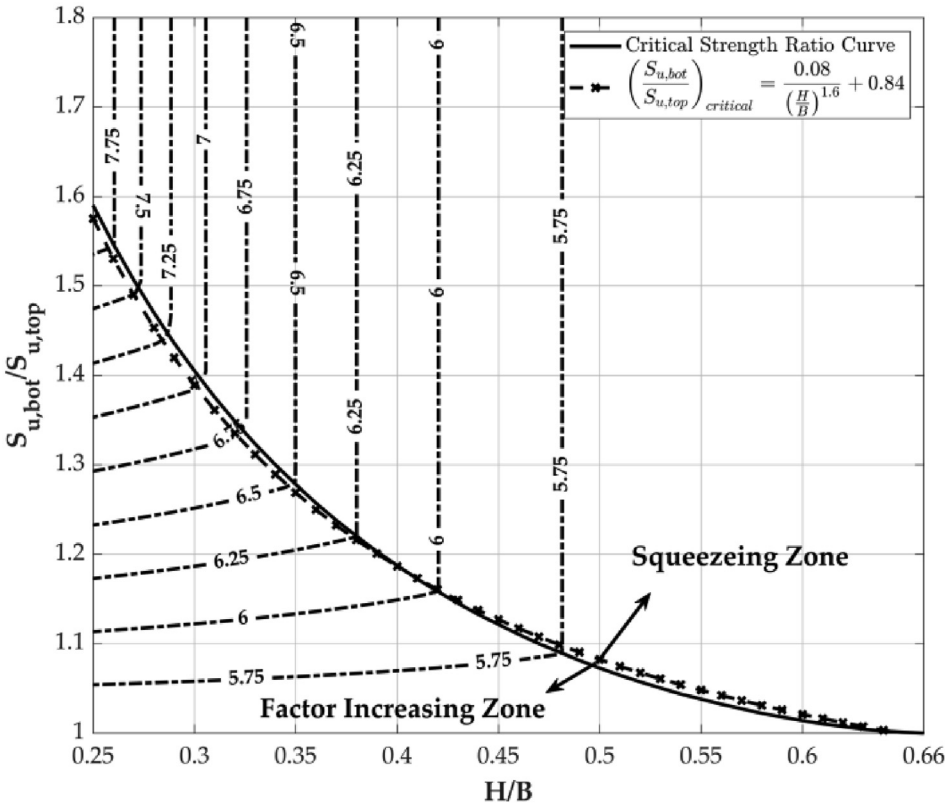

Fig. 10. Contours of the bearing factor surface on $S_{u,bot}/S_{u,top} \geq 1$ side.

mechanisms to evaluate the bearing capacity by assuming the strata line as a rigid base. However, it relies on engineering judgments regarding whether the in situ conditions satisfy the assumptions of a rigid base.

5. Numerical simulation results

To evaluate the bearing capacity of a surface footing resting on a double-layered soil system, closed-form and semi-empirical solutions have been proposed, and investigations based on numerical simulations have been performed. This study utilized a series of numerical simulations from FLAC to evaluate the bearing capacity of both perfectly rough and smooth footings on a double-layered soil system. For the homogeneous soil deposit case ($S_{u,bot}/S_{u,top} = 1.0$), the numerical solution is $N_c = 5.17$ for a perfectly rough footing and $N_c = 5.10$ for a perfect smooth footing. For a foundation on double-layered soils, the values of the bearing factors with various H/B and $S_{u,bot}/S_{u,top}$ are shown in Figs. 11 and 12 for perfectly rough and perfectly smooth footings, respectively. It can be observed from these figures: (I) while H/B maintains a constant value, N_c increases as the strength ratio ($S_{u,bot}/S_{u,top}$) increases until reaching the critical strength ratio; (II) the bearing factor is more sensitive to $S_{u,bot}/S_{u,top}$ for the smaller normalized layer thickness; (III) on $S_{u,bot}/S_{u,top} \leq 1.0$ side, the foundation roughness effect on N_c is not distinct. Compared to the behaviors of the bearing factors shown in Figs. 11 and 12, the results from the rotational mechanism (Fig. 5) are close to but higher than those for a perfectly rough footing, and they increase linearly before reaching plateau values on n > 0 side.

The bearing factor surface of the perfectly rough strip footings computed from the FLAC simulations is shown in Fig. 13, and Fig. 11 shows its side view from the strength ratio. The characteristics of the N_c surface of a perfectly rough footing are similar to those of a perfectly smooth footing; therefore, only the results of the perfectly rough footing are presented here. Similar to the behaviors shown in Fig. 7, for $S_{u,bot}/S_{u,top} < 1.0$ side, the bearing factors may be equal to or less than those of a footing on a homogeneous soil deposit. However, for $S_{u,bot}/S_{u,top} > 1.0$, an increment in N_c only occurs for $H/B \leq 0.7$.

5.1. A surface footing on a $S_{u,bot}/S_{u,top} > 1.0$ soil system

When the foundation is placed on a weaker stratum overlying a stronger stratum system ($S_{u,bot}/S_{u,top} > 1.0$), the normalized stratum thickness

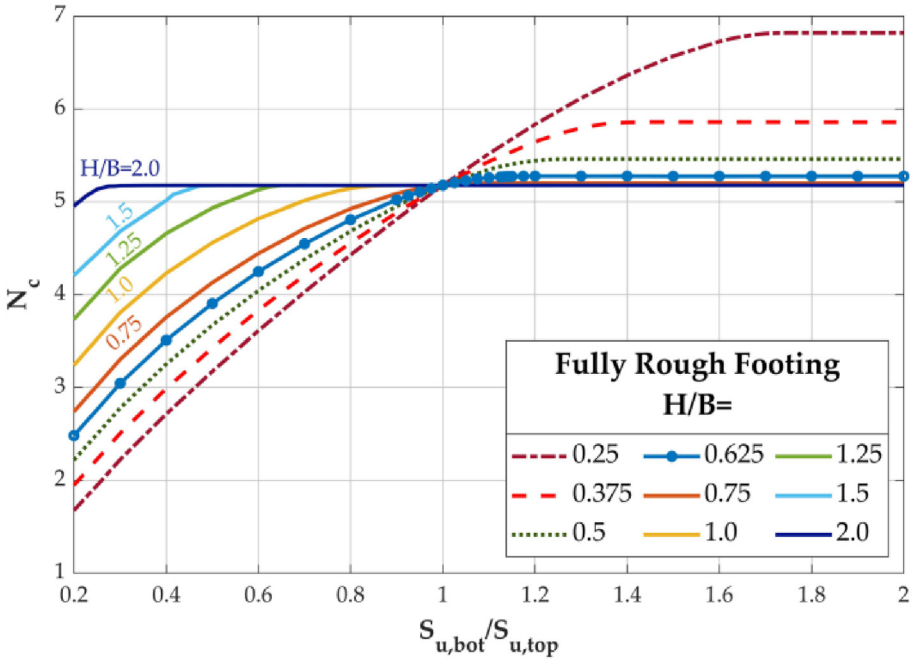

Fig. 11. Bearing factor N_c of perfectly rough strip footings from FLAC simulations.

is the main factor that determines whether the bearing factor increases. The subsequent soil layer strength has no effect on the foundation capacity for larger H/B and the associated bearing factor would maintain a constant value, such as $N_c = 5.17$ for a perfectly rough footing and $N_c = 5.10$ for a perfectly smooth footing. In contrast, for a smaller normalized layer thickness, the ultimate bearing capacity was affected by the stronger bottom soil deposit until squeezing occurred. Similar to the results for the rotational mechanism, the bearing factor increased as the strength ratio ($S_{u,bot}/S_{u,top}$) increased until a critical strength ratio was reached.

Critical strength ratio results for perfectly rough and smooth footings from FLAC simulations on $S_{u,bot}/S_{u,top} \geq 1.0$ side are shown in Fig. 14. The trend

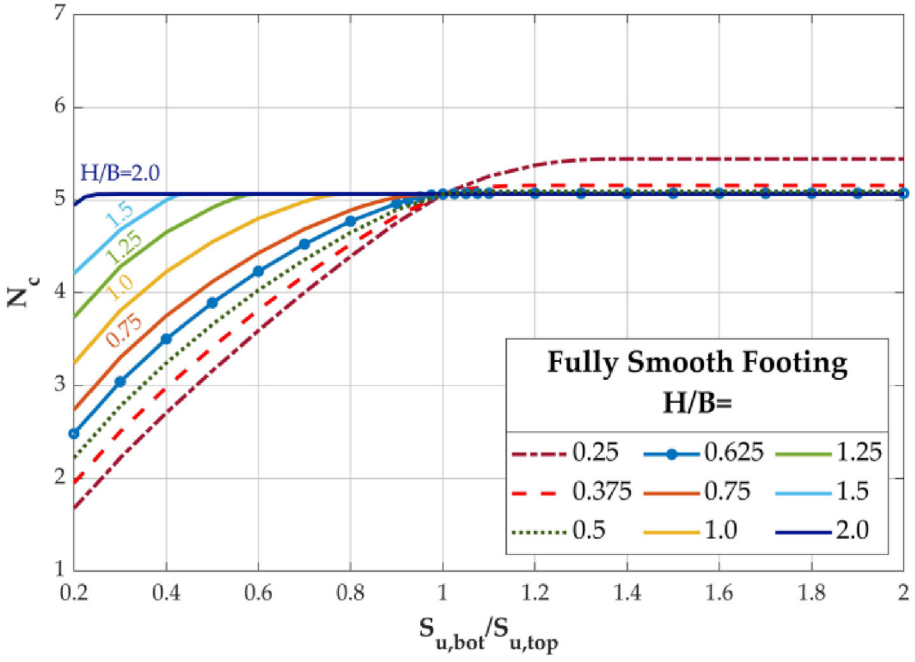

Fig. 12. Bearing factor N_c of perfectly smooth strip footings from FLAC simulations.

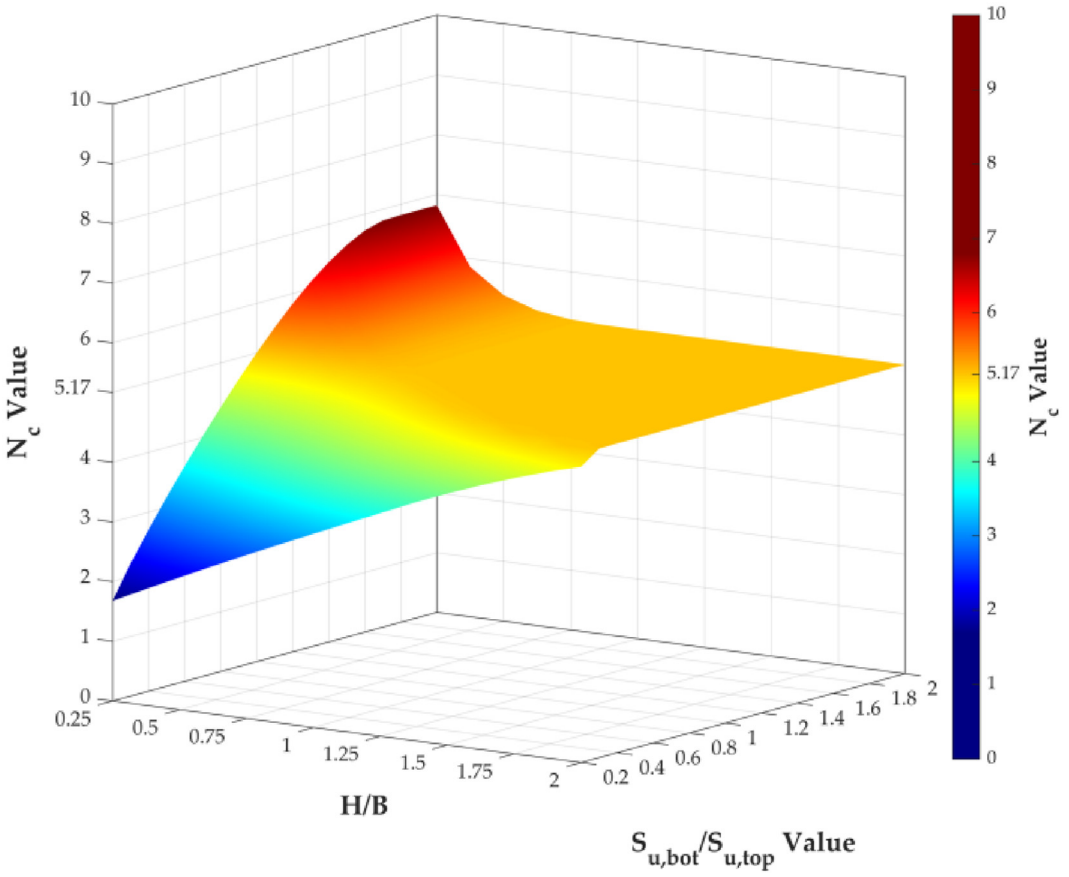

Fig. 13. Bearing factor surface of perfectly rough footings computed from FLAC simulation.

of the perfectly rough footing data matches that of the curve computed from the rotational mechanism; however, the values are slightly higher. Although the trend of the perfectly smooth footing data is close to that of the others, the effect of the foundation roughness on the values is significant. The abscissa values of the intersection points of the critical strength ratio results and the horizontal line $S_{u,bot}/S_{u,top} = 1.0$ indicates the required maximum H/B for different footing roughness or failure mechanisms for topsoil stratum squeezing. Similar to the characteristic zones shown in Figs. 8 and 10, soil squeezing occurs if the coordinates of the initial soil-strength ratio and normalized layer thickness are in Zone (I). Therefore, an increment in bearing factor, squeezing mechanism, occurs up to $H/B \leq 0.7$ for a perfectly rough footing, $H/B \leq 0.66$ obtained by rotational mechanism, and $H/B \leq 0.5$ for a perfectly smooth footing. In addition, the results from the rotational mechanism were much closer to the perfectly rough footing condition, as shown in Fig. 14.

Because the bearing factor surfaces and critical strength ratio results from the rotational mechanism and FLAC simulations are similar, it can be inferred that the bearing factor characteristics should be similar for both methods. For a certain H/B, the bearing factor increased as the strength ratio increased in Zone (II) and then plateaued in Zone (I). As shown in Fig. 15, the associated squeezing failure mechanism was entirely constrained in the topsoil stratum; therefore, the foundation capacity was independent of the bottom-stratum soil strength.

The bearing factors in Zones (I) and (II) are significantly affected by the footing roughness from the FLAC simulation results; however, the effect decreases as the H/B increases. For instance, the value of a perfectly rough footing is approximately 35% greater than that of a perfectly smooth footing at $H/B = 0.25$. However, when the normalized layer thickness increased to $H/B = 0.5$, the difference decreased to approximately 12%.

Although the exact solutions of bearing factors of a foundation on a homogeneous cohesive soil layer computed from Prandtl and Hill are identical, $\pi + 2$, the assumed failure mechanisms of the two methods are different. However, the failure mechanism of a footing in a double-layered soil system changes with the strength ratio, normalized layer

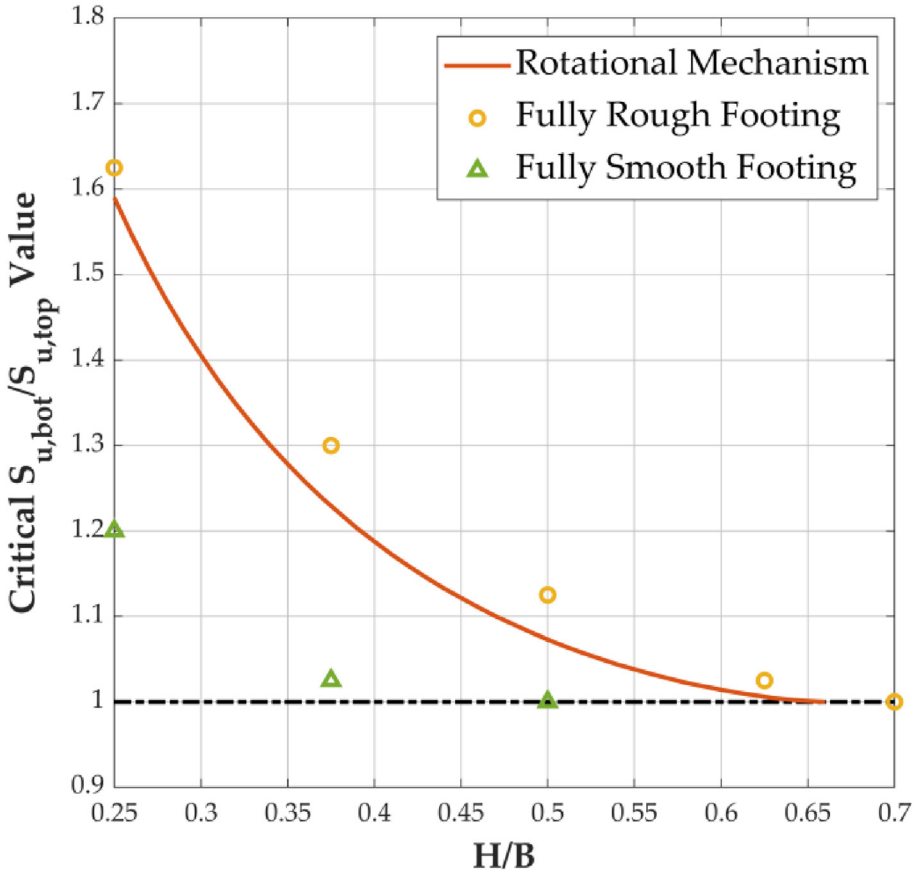

Fig. 14. Critical strength ratio results for perfectly rough and smooth footings from FLAC simulations on $S_{u,bot}/S_{u,top} \geq 1$ side.

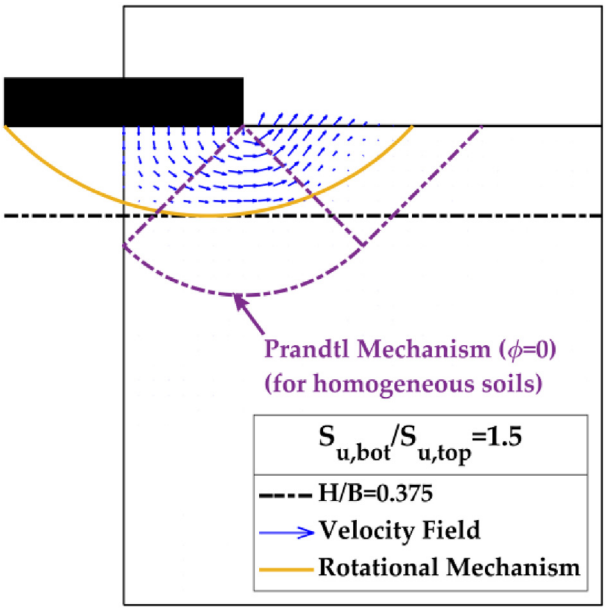

Fig. 15. Squeezing failure mechanisms of a perfectly rough footing from FLAC and rotational mechanism.

thickness, and footing roughness. For a perfectly smooth footing in the squeezing zone, the associated velocity field at the numerical limit load is closer to the Hill Mechanism than to the Prandtl Mechanism (Fig. 16). The differences in the bearing factors shown in Figs. 11 and 12 indicate different failure mechanisms under different footing roughness conditions.

5.2. A surface footing on a $S_{u,bot}/S_{u,top} < 1.0$ soil system

Based on the numerical simulation results (Figs. 11 and 12), the bearing factors on the $S_{u,bot}/S_{u,top} < 1.0$ side were affected slightly by the footing roughness. Fig. 17 shows the results of the critical strength ratio obtained from the rotational mechanism, FLAC simulations, including perfectly rough footing and perfectly smooth footing, and SNAME [19]. It can be observed from this figure that (I) all critical strength ratios decreased as H/B increased. It can be inferred that the subsequent weaker layer has less influence on the bearing factor for the larger normalized layer thickness. (II) The difference between perfectly

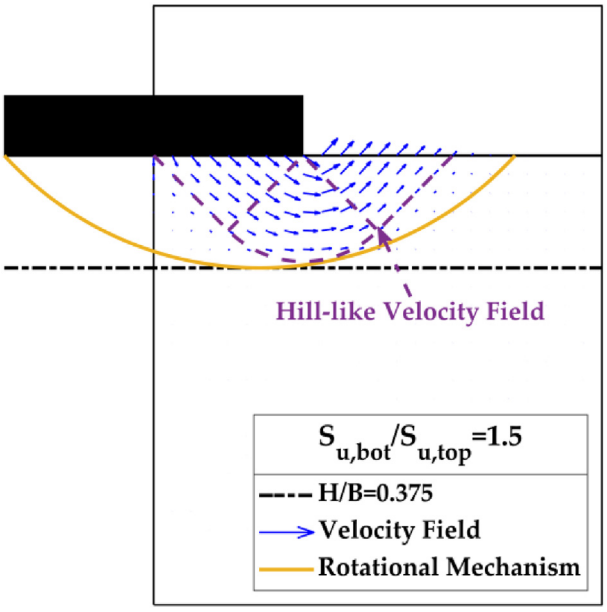

Fig. 16. Squeezing failure mechanisms of a perfectly smooth footing from FLAC and rotational mechanism.

rough footing cases and perfectly smooth footing cases is slight. It implies that the failure mechanisms of two roughness conditions are also similar. (III) For $H/B \leq 0.9$, the results determined by the rotational mechanism are very close to those from the numerical simulations. However, as the normalized layer thickness increases, the difference becomes more significant. In addition, the size of Zone (III) can be determined using a rotational mechanism, FLAC simulations, and SNAME [19] method. Applying different methods results in varying sizes of Zone (III), with the order of sizes being FLAC simulations > rotational mechanism > SNAME method. This zone determined by the SNAME [19] method can only contain approximately four points of the test data (17.4 %) from Brown and Meyerhof [26]; therefore, it is less conservative to apply the SNAME method to predict the range of the bearing factor decreasing zone.

Fig. 17 shows that the trend of the FLAC data is similar to that of the curve computed from the

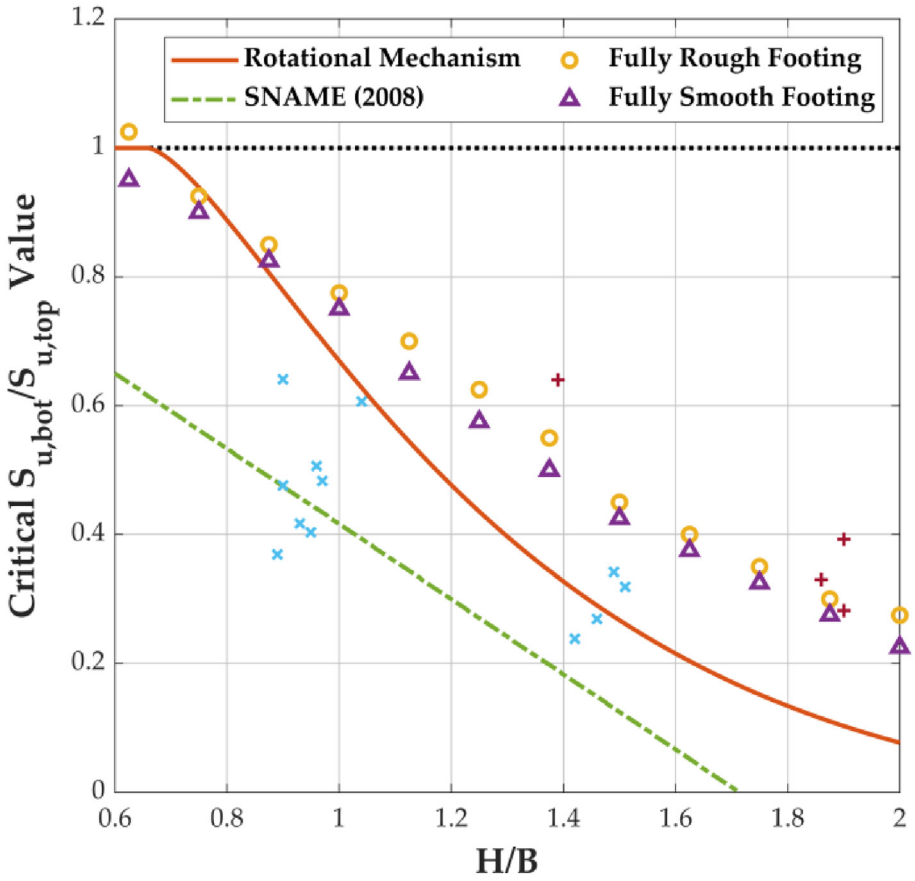

Fig. 17. Critical strength ratio results for perfectly rough and smooth footings from FLAC simulations on $S_{u,bot}/S_{u,top} \leq 1$ side and testing data from Brown & Meyerhof [26].

rotational mechanism. The zone definitions shown in Fig. 8 indicate that the characteristics of the bearing factors above the critical strength ratio simulation data maintain constants, 5.17 for a perfectly rough footing and 5.10 for a perfectly smooth footing; however, it decreases with departure from the critical strength ratio data in Zone (III). It is much more valuable to investigate the boundary curve between Zones (III) and (IV) for a surface footing on double-layered soils because catastrophic disasters may occur if the soil-foundation system is far away from the boundary in Zone (III).

The bearing factor in Zone (III) decreases with departure from the critical strength ratio curve, however, the associated soil plastic flow range increases. Terzaghi [14] and Vesic [34] indicated that the possible foundation failure modes were general shear, local shear, and punching shear failure. Merifield et al. [28] and Merifield and Nguyen [35] divided punching shear failure into partial and full punching shearing failures. Although the bearing factor attempts to decrease by moving the boundary curve backward in Zone (III), the demarcation between the partial punching shearing failure and full punching shearing failure is not distinct from the bearing factor figures, as shown in Figs. 11 and 12.

According to the numerical results, the soil-foundation interface condition had little influence on the critical strength ratio, and the difference in N_c values between the two extreme conditions was approximately 2%. As mentioned above, the failure mechanisms of the two roughness conditions were very similar for $S_{u,bot}/S_{u,top} < 1.0$; however, they changed with various strength ratios and normalized layer thicknesses. Fig. 18 shows the velocity field of a perfectly rough footing at the numerical collapse load, where $H/B = 0.625$ and $S_{u,bot}/S_{u,top} = 0.7$. The soil plastic flow pattern was similar to the Prandtl Mechanism for homogeneous soils; however, the range of the field was larger. Nevertheless, when the difference between the two strata strengths is large, such as $S_{u,bot}/S_{u,top} = 0.2$, as shown in Fig. 19, the soil plastic flow pattern is similar to the punching shear failure mechanism proposed by Meyerhof [36]. The following features can be observed from the simulation results: (I) the footing and the top-layered soil underneath it attempt to penetrate downward into the subsequent layer, and the affected soil plastic flow range in the bottom stratum is much larger than that of the homogeneous soils; (II) the top-layered soil neighboring the foundation have a smaller velocity field, and the soil state is still elastic; and (III) the velocity field of the top-stratum soils next to the elastic zone is distributed approximately upward; therefore, the ground surface may bulge during footing penetration.

6. Discussion

To evaluate the bearing capacity correctly, foundation failure mechanisms should be thoroughly investigated. The failure pattern of the rotational mechanism is one-sided (asymmetric) in contrast to Prandtl's [21] or Terzaghi's [14] symmetrical plastic soil-flow patterns. However, the bearing factor characteristics of a foundation on double-layered cohesive soils determined by the rotational mechanism were similar to those estimated from the FLAC simulations. The features of N_c can be categorized by the bearing factor characteristic chart, which includes four zones with associated failure

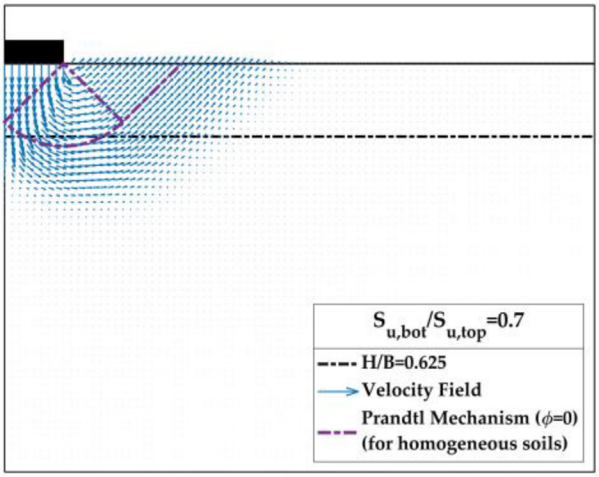

Fig. 18. Soil plastic flow pattern of a footing on $S_{u,bot}/S_{u,top} = 0.7$ and $H/B = 0.625$ double-layered soil conditions.

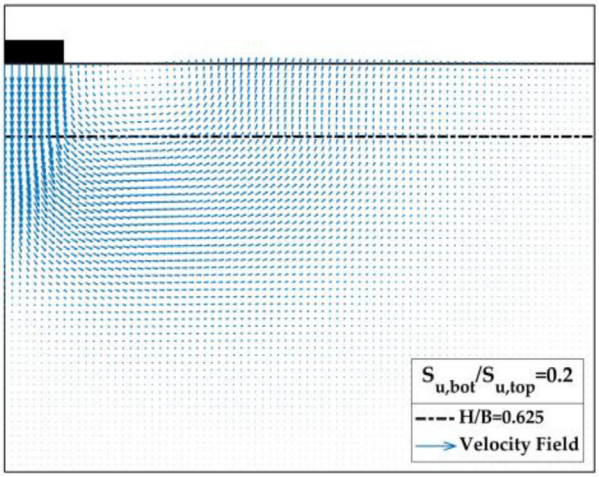

Fig. 19. Soil plastic flow pattern of a footing on $S_{u,bot}/S_{u,top} = 0.2$ and $H/B = 0.625$ double-layered soil conditions.

mechanisms. The first step of the double-layered footing capacity evaluation is to determine the appropriate zone of the soil-foundation problem. The regression equations provide a good reference for a rapid evaluation in practical applications. Furthermore, the assumed foundation failure mode should be similar to the failure mechanism of the actual engineering problems, and the one-sided sliding mode may be more suitable for certain engineering problems. For example, the soil flow pattern of the spudcan footings of jack-up barges during the preloading stage can be described well by Meyerhof's bearing capacity theory (adopted in SNAME) because all legs penetrate into the soil evenly. It can be inferred that the failure mode of each footing was symmetric. Nevertheless, it may be closer to one-sided sliding for a specific leg of the jack-up barge when the punch-through shear failure occurs. Most failure modes for spread footings are probably one-sided sliding owing to nonhomogeneous or uneven soil conditions.

Appropriate estimation of the bearing capacity is an important issue in geotechnical engineering. Because the dimensions of offshore foundations are generally larger than those of onshore foundations, it is necessary to consider the effects of layered soils in bearing capacity assessments. The bearing factors of a footing on a double-layered cohesive soil profile were investigated in this study, and their characteristics are described by Zones (I) to (IV), as shown in Fig. 8. If the normalized layer thickness (H/B) is relatively small and the strength ratio is $S_{u,bot}/S_{u,top} > 1.0$, the associated bearing factor is located in Zone (I) or (II). While H/B remains constant, N_c increases as $S_{u,bot}/S_{u,top}$ increases until it reaches the critical strength ratio. Note that the bearing factors in Zone (I) are a function of the normalized layer thickness, and the associated soil slip circle or range of the plastic soil flow pattern is completely constrained in the weaker topsoil stratum. In contrast, the bearing factors in $S_{u,bot}/S_{u,top} < 1.0$ side might be smaller than that of the homogeneous case, and the phenomenon of a reduction in bearing capacity is much more valuable to investigate because catastrophic disasters may occur if the soil-foundation system is far away from the boundary in Zone (III). Although the failure mechanisms may include partial and full punching shearing failures, their demarcation is not distinct from the results of the bearing factor variations. From the numerical simulation results, the range of the failure mechanism for $S_{u,bot}/S_{u,top} > 1.0$ condition attempts to shrink compared with that of homogeneous soils; however, it increases for $S_{u,bot}/S_{u,top} < 1.0$ condition. The same phenomena were also observed in the rotational mechanism [8]; therefore, a wider range of soil properties should be considered for a footing on a stronger layer overlying a softer layer system.

7. Conclusions

The bearing capacity of footings set on a double-layered cohesive soil profile was investigated, and the results and highlights of the rotational mechanism and FLAC numerical simulation are as follows:

1. Although the failure pattern of the rotational mechanism is a one-sided sliding surface, which is different from Prandtl's [21] or Terzaghi's [14] symmetrical plastic soil flow patterns, the associated bearing factor characteristics of a foundation on a double-layered cohesive soil system are similar to those obtained from the FLAC simulations.
2. For a specific site, engineers are aware that the strength ratio ($S_{u,bot}/S_{u,top}$), thickness of the top layer (H), and width of the foundation (B) must be determined. However, as the width of the foundation (B) increases or the normalized layer thickness (H/B) decreases, the N_c value becomes equal to that under homogeneous conditions until it reaches the minimum foundation size required to consider the layered soil effect. This study provides dimensionless results, including a graphical representation of the relationship (Fig. 8) and regression forms, to distinguish the bearing factor characteristics.
3. Considering the footing on a weaker stratum overlying a stronger stratum system ($S_{u,bot}/S_{u,top} \geq 1.0$), the condition in which the N_c value might be greater than that of homogeneous soil will occur when $H/B \leq 0.66$ determined by rotational mechanism, $H/B \leq 0.7$ for a perfectly rough footing and $H/B \leq 0.5$ for a perfectly smooth footing. In addition, if the bearing factor belongs to Zone (I), the associated soil slip surface or plastic soil flow is fully constrained in the weaker top soil layer.
4. When foundations are placed on a stronger stratum overlying a weaker stratum system ($S_{u,bot}/S_{u,top} \leq 1.0$), there might be a reduction in bearing factor, which is located in Zone (III), and the associated slip circular failure surface or the range where soils occur plastic flow may enlarge. Additionally, the results obtained by applying the SNAME [19] method to predict the range of Zone (III) were the least conservative among all methods.
5. Based on the FLAC simulation, the bearing factor on $S_{u,bot}/S_{u,top} \geq 1.0$ side is more affected by

the foundation roughness than that on $S_{u,bot}/S_{u,top} \leq 1.0$ and the effect would decrease as the H/B increases.

Conflict of interest

The authors declare that there is no conflict of interest.

Acknowledgements

This research presented here was supported by the following grants: Increasing the Ultimate Holding Capacity of Marine Plate Anchors by Keying Process (NSTC 112-2221-E-035-055-), Investigations of Ultimate Bearing Capacity and Associated Soil Plastic Flow of Jack-up Barge Foundations in Layered Soils (MOST 111-2221-E-035-030), and Risk Assessment of Floating Offshore Wind Turbine Anchor Foundation Design and Installation (MOST 110-2622-E-006-026- & MOST 111-2622-E-006-028-), the National Science and Technology Council of Taiwan.

References

[1] Leithead WE. Wind energy. Phil. Trans. R. Soc. A. 2007;365:957−70.
[2] Olsen F, Dyre K. Vindeby off-shore wind farm - construction and operation. Wind Eng 1993;17:120−8.
[3] Lin Der-Guey, Wang Sheng-Hsien, Chou Jui-Ching, Ku Cheng-Yu, Chien Lien-Kwei. Numerical analyses of pile foundation for support structure of offshore wind turbine at changhua coast in Taiwan. J Mar Sci Technol 2020;28.
[4] Chi CM, Lin ZS. The footing size effect on punch-through bearing capacity assessment of jack-up barges in Western Taiwan offshore layered soil. In: The 30th international ocean and polar engineering conference. Shanghai, China: The International Society of Offshore and Polar Engineers; 2020. page ISOPE-I-20-2223.
[5] Dean ETR. Offshore geotechnical engineering: principles and practice. London : Reston, VA: Thomas Telford ; ASCE Press [distributor]; 2010.
[6] Randolph MF, Gourvenec S. Offshore geotechnical engineering. London ; New York: Spon Press; 2011.
[7] Clausen CJF, Dibiagio EJF, Duncan JM, Andersen KH. Observed behavior of the Ekofisk oil storage Tank foundation [Internet]. In: Offshore Technology conference. Houston, Texas: Offshore Technology Conference; 1975 [cited 2020 Oct 30]. Available from: http://www.onepetro.org/doi/10.4043/2373-MS.
[8] Chi CM, Lin ZS. The bearing capacity evaluations of a spread footing on single thick stratum or two-layered cohesive soils. JMSE 2020;8:853.
[9] Davis EH, Booker JR. The effect of increasing strength with depth on the bearing capacity of clays. Geotechnique 1973;23:551−63.
[10] Hossain MS, Kim Y, Zheng J. Installation of spudcans [Internet]. In: Cui W, Fu S, Hu Z, editors. Encyclopedia of ocean engineering. Singapore: Springer Singapore; 2021 [cited 2023 Mar 7]. page 1−19.Available from: http://link.springer.com/10.1007/978-981-10-6963-5_205-1.
[11] Le Tirant P. Seabed reconnaissance and offshore soil mechanics for the installation of petroleum structures. Paris: Technip; 1979.
[12] Menzies D, Lopez CR. Four atypical jack-up rig foundation case histories. In: The 13th international conference on the jack-up platform: design, construction and operation; 2011. London.
[13] Murff JD. Estimating the capacity of offshore foundations. In: Offshore site investigation and geotechnics: integrated technologies - present and future. London, UK: Society of Underwater Technology; 2012.
[14] Terzaghi K. Theoretical soil mechanics. New York: John Wiley and Sons; 1943.
[15] Lin Der-Guey, Liu Wen-Tsung, Chou Jui-Ching. Load Transfer and deformation analyses of piled-raft foundation in Taipei metropolitan. J Mar Sci Technol 2016;24.
[16] Lin Der-Guey, Liu Wen-Tsung, Chou Jui-Ching. Mechanical behaviors of piled-raft foundation and diaphragm Wall in deep excavation of Taipei metropolitan. J Mar Sci Technol 2016;24.
[17] Das BM. Principles of foundation engineering. Eight edition. Boston, MA: Cengage Learning; 2016.
[18] Meyerhof GG. Some recent research on the bearing capacity of foundations. Can Geotech J 1963;1:16−26.
[19] SNAME. Guidelines for site specific assessment of mobile jack-up units [internet]. Society of Naval Architects and Marine Engineers; 2008. Available from: https://books.google.com.tw/books?id=Tij_swEACAAJ.
[20] Gui MW, Muhunthan B. Bearing capacity of foundations on sand using the method of slip line [cited 2023 Aug 1] Journal of Marine Science and Technology [Internet] 2006;14. Available from: https://jmstt.ntou.edu.tw/journal/vol14/iss1/1.
[21] Prandtl L. Hauptaufsätze: Über die Eindringungsfestigkeit (Härte) plastischer Baustoffe und die Festigkeit von Schneiden. Z Angew Math Mech 1921;1:15−20.
[22] Hill R. The mathematical theory of plasticity [internet]. Clarendon Press; 1950. Available from: https://books.google.com.tw/books?id=Ti-bcsBkVAMC.
[23] Zhang W, Zhou Z, Pradhan DL, Wang P, Jin H. Design considerations of drag anchors in cohesive soil for floating facilities in the South China sea. Mar Struct 2022;81:103101.
[24] Hwang JH, Wang JS. A comparative study on the calculation methods of axial bearing capacity of foundation piles for offshore wind turbines: (I) uniform soil layers. Sino-Geotechnics 2022:95−106.
[25] Reddy AS, Srinivasan RJ. Bearing capacity of footings on layered clays. J Soil Mech Found Div 1967;93:83−99.
[26] Brown JD, Meyerhof GG. Experimental study of bearing capacity in layered clays. In: Proceedings of the 7th international conference on soil mechanics and foundation engineering. Mexico: International Society for Soil Mechanics and Geotechnical Engineering; 1969. page 45−51.
[27] Chen WF. Limit analysis and soil plasticity. Amsterdam ; New York: Elsevier Scientific Pub. Co; 1975.
[28] Merifield RS, Sloan SW, Yu HS. Rigorous plasticity solutions for the bearing capacity of two-layered clays. Geotechnique 1999;49:471−90.
[29] Meyerhof GG, Hanna AM. Ultimate bearing capacity of foundations on layered soils under Inclined load. Can Geotech J 1978;15:565−72.
[30] Lambe TW, Whitman RV. Soil mechanics. New York: Wiley; 1969.
[31] Cheng P, Guo J, Yao K, Liu C, Liu X, Liu F. Uplift behavior of pipelines buried at various depths in spatially varying clayey seabed. Sustainability 2022;14:8139.
[32] Itasca Consulting Group, Inc. FLAC — fast Lagrangian analysis of continua. 2019.
[33] Shield RT. The plastic indentation of a layer by a flat punch. Q Appl Math 1955;13:27−46.
[34] Vesić AS. Analysis of ultimate loads of shallow foundations. J Soil Mech Found Div 1973;99:45−73.
[35] Merifield RS, Nguyen VQ. Two- and three-dimensional bearing-capacity solutions for footings on two-layered clays. Geomechanics Geoengin 2006;1:151−62.
[36] Meyerhof GG. Ultimate bearing capacity of footings on sand layer overlying clay. Can Geotech J 1974;11:223−9.